PCCP

Accepted Manuscript

ROYAL SOCIETY OF CHEMISTRY

www.rsc.org/pccp

Determination of accurate electron chiral asymmetries in fenchone and camphor in the VUV range: sensitivity to isomerism and enantiomeric purity†

Laurent Nahon[a,*], Lipsa Nag[a], Gustavo A. Garcia[a] , Iuliia Myrgorodska[a,b], Uwe Meierhenrich[b], Samuel Beaulieu[c], Vincent Wanie[c], Valérie Blanchet[c], Romain Géneaux[d] and Ivan Powis[e]

[a] *Synchrotron SOLEIL, L'Orme des Merisiers, St. Aubin BP 48, 91192 Gif sur Yvette, France*
E-mail : *laurent.nahon@synchrotron-soleil.fr*
[b] *Institut de Chimie de Nice, UMR 7272 CNRS, University Nice Sophia Antipolis, 28 avenue Valrose, 06108 Nice, France.*
[c] *Université de Bordeaux-CNRS-CEA, CELIA, UMR 5107, 33405 Talence, France*
[d] *CEA, IRAMIS-LIDyL, CEA-Saclay, 91191 Gif sur Yvette , France*
[e] *School of Chemistry, University of Nottingham, Nottingham NG7 2RD, UK*

Photoelectron circular dichroism (PECD) manifests itself as an intense forward/backward asymmetry in the angular distribution of photoelectrons produced from randomly-oriented enantiomers by photoionization with circularly-polarized light (CPL). As a sensitive probe of both photoionization dynamics and of the chiral molecular potential, PECD attracts much interest especially with the recent performance of related experiments with visible and VUV laser sources. Here we report, by use of quasi-perfect CPL VUV synchrotron radiation and using a double imaging photoelectron/photoion coincidence (i^{2}PEPICO) spectrometer, new and very accurate values of the corresponding asymmetries on showcase chiral isomers: camphor and fenchone. These data have additionally been normalized to the absolute enantiopurity of the sample as measured by a chromatographic technique. They can therefore be used as benchmarking data for new PECD experiments, as well as for theoretical models. In particular we found, especially for the outermost orbital of both molecules, a good agreement with CMS-Xα PECD modeling over the whole VUV range. We also report a spectacular sensitivity of PECD to isomerism for slow electrons, showing large and opposite asymmetries when comparing R-camphor to R-fenchone (respectively -10% and +16 % around 10 eV). In the course of this study, we could also assess the analytical potential of PECD. Indeed, the accuracy of the data we provide are such that limited departure from perfect enantiopurity in the sample we purchased could be detected and estimated in excellent agreement with the analysis performed in parallel via a chromatographic technique, establishing a new standard of accuracy, in the ±1 % range, for enantiomeric excess measurement via PECD. The i^{2}PEPICO technique allows correlating PECD measurements to specific parent ion masses, which would allow its application to analysis of complex mixtures.

†Electronic supplementary information (ESI) available: Compilation of literature values, and those obtained in this work of the mean $b_1^{(+1)}$ values for ionization from the HOMO and HOMO-1 orbitals of 1R-4R-(+)-camphor; compilation of literature values, and those obtained in this work of the mean $b_1^{(+1)}$ values for ionization from the HOMO orbital and A band of 1R-4S-(–)-fenchone; observed enantiomeric excesses ratio for camphor and fenchone at the photon energies where both enantiomers were measured; computed isosurface plots showing the electronic density for the HOMO orbitals of 1R,4R-camphor and 1R,4S-fenchone.

View Article Online
DOI: 10.1039/C6CP01293K

1. Introduction

Since its formal prediction in 1976 [1], its first precise calculated values in 2000 [2, 3], and its first experimental evidence in 2001 [4], Photoelectron Circular Dichroism (PECD) has been the subject of a large number of both theoretical and experimental studies [5-7], mainly carried out with Synchrotron Radiation (SR), for valence and core-shell ionization. PECD is an orbital-specific chiroptical effect which manifests itself as a forward/backward asymmetry, with respect to the photon axis, of the electron angular distribution produced by the photoionization with Circularly Polarized Light (CPL) of randomly-oriented pure enantiomers of a chiral system. More precisely, PECD asymmetry can be defined, for a given light helicity and molecular handedness, as the normalized difference between the electron flux in the forward vs backward direction which will equal $2b_1$ in the case of one-photon ionization, where b_1 is the so-called dichroic parameter. The corresponding asymmetry factors are large (up to a few tens of %) because PECD emerges in the pure electric-dipole approximation, and PECD is therefore orders of magnitude more intense than other chiroptical probes, such as circular dichroism in absorption, requiring interaction with weaker (magnetic and quadrupolar) terms. [8] As found for other chiroptical parameters, b_1 is anti-symmetric with the switching of either enantiomers or light helicity.

In the context of molecular photoionization, b_1 depends on both the initial-state (orbital) and final state (continuum) [9, 10]. However, unlike the usual cross section σ or the asymmetry parameter β, this new observable has a pure quantum origin in the scattering of the outgoing electron by an intrinsically chiral potential, being also fully dependent on the sine of the relative phase between adjacent outgoing partial wave continuum functions [5]. This phase dependence makes b_1 a very sensitive probe of the whole molecular potential, much more so than σ or β, with a demonstrated dependence on conformers [11-15], chemical substitution [16, 17], dimerization [18] and clustering [19, 20], and even vibrational-dynamics [21, 22].

PECD possesses, therefore, a real analytical potential in the gas phase (i.e. in a solvent-free environment) which has recently been the driving force for a new emerging field of table-top PECD experiment based on fs laser ionization: UV-Resonance-enhanced multi-photon ionization (REMPI) PECD[23-28] or 1-photon VUV PECD by High Harmonic Generation (HHG) [29]. These experiments are paving the way towards a potentially very sensitive analytic use of PECD for enantiomeric separation on mass-selected samples [30], competing with other promising and emerging enantiomeric probes in the gas phase such as the one based upon phase-sensitive microwave spectroscopy [31-33]. A natural step further will be the development of Time-Resolved (TR)-PECD to probe stereo-chemical reactions of chiral systems in real time.

Most of the pioneering SR-based experiments [34-36] as well as the new generation of laser-based PECD experiments, were performed on the monoterpenes camphor and/or fenchone [24-26, 30, 37], two isomeric forms of a rigid, single-conformer, bi-cyclic ketone, quite easy to bring in the gas phase, and that can both be considered as showcases for molecular chirality. Note that fenchone has also been used to demonstrate a pioneering chiroptical method based upon High Harmonic Generation (HHG) from a chiral molecule [38], and both isomers have been studied by REMPI-UV Ion Yield CD [39]. To be validated in

View Article Online
DOI: 10.1039/C6CP01293K

sensitivity and reliability laser-based PECD experiments need benchmarking with data obtained with more well-established and controlled experiments such as the one that can be carried out with pure-CPL SR sources. This is one of the motivations for the present study, which provides for the first time complete and very accurate measurements of b_1 parameters for the two outermost orbitals of camphor and fenchone up to hν ~ 16 eV. Indeed, in the past some of us [34, 36, 40] and other authors [35] published some data for these molecules but, because of technical SR light source limitations at the time, there were uncovered regions of the spectrum — notably in the crucial 10 to 15 eV photon energy range for which theoretical models [36, 41] predict large oscillations of b_1. The benchmarking of theory versus experiment, in this specific range, with very accurate data obtained with a state-of-the-art double imaging electron/ion coincidence (i^{2}PEPICO) spectrometer set-up and quasi-perfect CPL is the second motivation of the present study, especially in a context where multi-photon/high field PECD modeling has just been initiated on these showcase molecules [42, 43]. The precision of the measurements we provide are such that departures from perfect enantiopurity in the sample we purchased could be detected, quantified, and corrections applied to the measured b_1 parameter, all perfectly corroborated by an independent analysis performed via chromatographic techniques. Establishing this new standard of accuracy, in terms of enantiomeric excess measurement via PECD, became an important issue that we also focused on in the course of the data analysis.

Finally, and this is an important goal of this work, the observation of PECD for various valence orbitals for both fenchone and camphor, which only differ by the position of two methyl groups, will allow us to expand our previous knowledge[40] on the sensitivity of valence-shell PECD to isomerism which in this case cannot be detected from the shape of the photoelectron spectra.

2. Experimental Methods

Both R- and S-fenchone and R- and S-camphor were obtained from Sigma-Aldrich with a chemical purity above 98 %. In the case of fenchone, the optical rotations quoted in the bottle labels for both enantiomers ($[\alpha]_D^{24} = -50.5°$ for the R and $[\alpha]_D^{20} = +62°$ for the S) suggested a difference in enantiopurity, with an R/S ratio of 0.81. For camphor, the optical rotations quoted in the chemical analysis of the particular lots used ($[\alpha]_D^{24} = +44.6°$ for the R and $[\alpha]_D^{20} = -43.5°$ for the S), led to an R/S ratio of 1.02. Therefore, we decided to analyze the exact enantiopurity of the purchased samples with multi-dimensional gas chromatography coupled to time-of-flight mass spectrometry (GC×GC-TOFMS) [44]. The GC×GC column set consisted of a Chirasil-Dex CB (for fenchone) or Hydrodex-β-6-TBDM (for camphor) primary column modulator-coupled to a DB Wax secondary column. Temperature program was adapted to archive maximum peak resolution. Secondary column was operated with 30 °C off-set. Modulation period of 3s was applied. Helium was used as carrier gas at a constant flow of $\bar{u}$ = 1 mL min^{-1}. Sample volumes of 1 µL were injected in the split mode at an injector temperature of 230 °C. The TOF-MS was operated at a storage rate of 150 Hz, with a 25−500 amu mass range. Data were acquired and processed with LECO Corp ChromaTOF™ software. Samples of *S*- and *R*-enantiomers with the concentration 10^{-3} M were injected several times in order to obtain statistically relevant e.e. values.

View Article Online
DOI: 10.1039/C6CP01293K

PECD experiments were performed on the SAPHIRS endstation[45] of the VUV synchrotron beamline DESIRS[46], at the French synchrotron facility SOLEIL. Each enantiomer of each molecule was directly placed into a temperature-controlled in-vacuum stainless steel oven. The reservoir was gently heated at 40°C and the resulting vapor was mixed with 0.5 bars of He and adiabatically expanded through a 70 μm nozzle. After traversing a differentially pumped chamber with two ϕ=1mm skimmers, the collimated molecular beam crossed the synchrotron radiation at a right angle.

Tailored polarized light was provided by the HU640 electromagnetic undulator of DESIRS, set in the so-called "pure CPL-mode" and monochromatised with the 200 lines/mm grating of the 6.65 m normal incidence monochromator. For photon energies below 15 eV, a gas filter upstream was filled with Kr or Ar to remove the high harmonics from the undulator[47]. The monochromator slits were merely set to avoid saturation of the charged particle detectors, providing energy resolutions between 6 meV at the lowest photon energy, and 11 meV at the highest. The full polarization ellipse, including the unpolarized component, was measured *in situ* at the sample level with a dedicated polarimeter[48], and was found to be quasi-purely circular, with absolute circular polarization rates (S_3) values of 0.99 ± 0.01 over the whole photon energy range[46] which we have used to normalize the experimental PECD values. Further and more complicated corrections to the PECD values due to S_1 and S_2 terms can be neglected in view of the polarization purity. In addition, the stability of S_3 over time is routinely confirmed by frequent polarimetry checks.

Electrons and ions formed in the interaction region are accelerated in opposite directions by a continuous electric field perpendicular to the molecular and synchrotron beams. A complete description of the DELICIOUS3 i^{2}PEPICO spectrometer used in this work and its performances has been reported elsewhere[45, 49]. Briefly, it consists of an electron velocity map imaging (VMI) analyser coupled to a modified ion Wiley-McLaren imaging spectrometer. Electron and ion arrivals are correlated in time and therefore the photoelectron VMI images can be obtained and filtered as a function of ion mass and translational energy. Photoelectron spectra (PES) and angular parameters are then extracted from the Abel inversion of the VMI image using a least squares fitting of previously computed forward Abel functions[50] . For the PECD measurements, typically a total of around 20 images are obtained at a given fixed photon energy for a given enantiomer with alternating light helicities, switched every 15 min. The images are then summed according to the light helicity to provide a single pair composed of the left (LCP) and right (RCP) circularly polarized measurements. The PES is then obtained by Abel inversion of the LCP+RCP image with a kinetic energy resolution of 3% for the fastest electrons, while the $b_0 b_1$ term, where b_0 is the total cross-section of ionization of a given electronic band as given by the integral of the PES, is obtained from the LCP-RCP difference, leading to the final PECD, $2b_1$, through normalization by b_0 (see [36] for a complete description of the procedure). The statistical error bars are given as the standard error on the principle that each image pixel acts as an independent counter that follows a Poisson distribution, with the associated error properly propagated through all subsequent operations. Systematic errors are estimated by comparison of both enantiomers' data, which should exhibit perfect mirroring behavior.

3. Results and discussion

View Article Online
DOI: 10.1039/C6CP01293K

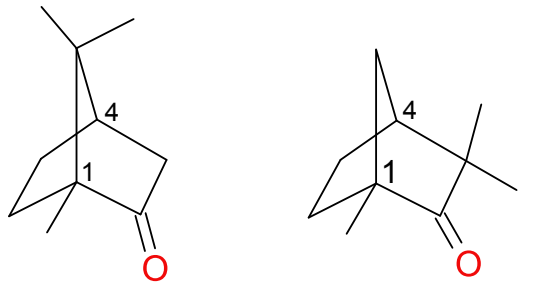

1R,4R camphor 1R,4S fenchone

Scheme 1: Structure of the camphor and fenchone molecules.

3.1 Camphor data

Figure 1 shows the typical data recorded in these experiments, in this case for R- and S-camphor at 12.3 eV. Several features mentioned in the introduction can be readily observed in the Figure. Indeed the large asymmetry observed with PECD up to 12% means that it is readily visible even in the raw non-inverted 2D- difference images shown in Figure 1a and 1b. The strong initial orbital dependency is also appreciated with the sign and magnitude changing for different electronic bands across the image radius. Moreover, the PECD value in Fig. 1c oscillates several times between IE=10 and 12 eV. These oscillations, although not seen in the VMI-PES concurrently recorded with our spectrometer, are real and exceed our error bars. They are perfectly mirrored in the R- and S- enantiomer curves as anticipated from the anti-symmetry of the b_1 coefficients for the two enantiomers , showing the high quality of the data. The mirroring is explored in Fig. 1d, by plotting the mean value or baseline
$BL = \frac{\mathrm{PECD_R}+\mathrm{PECD_S}}{2}$.
Deviation from the ideal value of zero could be ascribed to statistical error (different S/N), to systematic error (e.g. residual instrumental asymmetry), or to different enantiopurity. In the higher resolution PES recorded by Rennie et al.[51] with a hemispherical analyzer the electronic band structure is slightly more marked and seen to correlate with the PECD changes. The OVGF calculations published by Rennie et al. also correspond to the observed oscillations, which highlights the enhanced sensitivity of PECD to electronic structure when compared to usual observables such as ionization cross-sections — even in the case of congested electronic bands as already observed in camphor [36] and glycidol [13].

The onset of camphor parent ion fragmentation is ~9.7 eV, with the parent ion rapidly disappearing as photon energy is increased (less than 10% of parent yield remains at 10.0 eV). The first electronic band seen in Figure 1c, which corresponds to ionization of the HOMO orbital localized onto the carbonyl oxygen lone pair, results solely in the production of parent ion. Thus, by filtering the electron images according to the coincident parent ion mass, the electrons ejected from the HOMO can be better isolated. This becomes [36] extremely useful at high photon energies where the moderate resolution of the VMI leads to overlap between the HOMO and the inner orbital bands. Figure 2 illustrates the result of applying the filtering for the parent ions at $h\nu$=12.3 eV, and can be directly compared to Fig. 1. It is clear that the mass-filtering removes the contribution from inner orbitals since these lead to fragmentation. Conversely, to obtain the PECD of the deeper-lying orbitals, we have obtained the electron images correlated

View Article Online
DOI: 10.1039/C6CP01293K

to the fragment ions only, so ensuring removal of any contribution from the HOMO orbital electron data. This treatment is especially effective when the HOMO and HOMO-1 orbitals have b_1 parameters of opposite sign, and so might tend to cancel if unresolved, as happens here in certain regions of photon energy. For instance, at $h\nu$=12.3 eV the weighted HOMO $|b_1|$ values obtained from Fig. 1c (unfiltered) and Fig. 2 (filtered) are 0.055 and 0.058, respectively, a discrepancy in the unfiltered data of 5% due to the small overlap between HOMO and HOMO-1.

In addition, the double imaging coincidence scheme permits removing common background impurities such as water, N_2, O_2, which would increase the achiral content in the total signal used for normalization and therefore decrease the observed PECD. Overall, the procedure dramatically increases the signal-to-noise ratio with respect to previous non-coincident data[36, 40] recorded for camphor and fenchone, as evidenced with the low error bars and excellent mirror behavior. Indeed, in Figure 1c the PECD baseline, *BL*, barely deviates from the ideal zero value over the whole kinetic energy range, with a weighted mean value of 0.0003 ± 0.0005. Deviations from zero outside of the given error bars are ascribed to systematic errors. It is worth noting that the R and S measurements correspond to two different experiments spaced by one month. In Figure 2, the parent-coincident data show small deviations from perfect mirroring behavior, associated to the lower overall signal. Even in this case, however, the PES intensity weighted integral of the baseline, *BL*, over the FHWM of the HOMO band is very close to zero, 0.0005, so that the mean b_1 values across the HOMO and HOMO-1 regions (see text below and Figures 3 and 4) will have very similar absolute values for both enantiomers within the given error bars — provided both have the same enantiopurity.

However, at the photon energies where both enantiomers were recorded (12.3 and 15.0 eV), we initially found that the raw, uncorrected magnitude of the HOMO band PECD measured for the R enantiomer was slightly smaller than that of the S, leading to a $PECD_R$ / $PECD_S$ average ratio of 0.97 ± 0.02, as derived from the uncorrected data presented in Fig. S1(a). It is known that the magnitude of measured asymmetries will scale linearly with the absolute value of the enantiomeric excess (e.e.) as defined by ([R]-[S])/ ([R]+[S]) where [R] (resp. [S]) corresponds to the concentration of the R (resp. S) enantiomer, and this therefore suggests some variation of the relative enantiopurity of the two commercial samples with an e.e. ratio of 0.97 ± 0.02, surprisingly quite different from the value of 1.02 that could be inferred from the optical rotation data provided by Aldrich (see experimental methods above). We therefore took additional steps to verify purity of our samples analyzing them by chiral-sensitive GC×GC-TOFMS to obtain a precise value of the e.e. The results of the chromatographic analysis are shown in Table 1. The agreement between e.e. ratio deduced from these PECD data and the absolute e.e. obtained by GC×GC-TOFMS is remarkable, as are the experimental PECD error bars. The presented data of Fig.1, and that discussed further below discussed were subsequently corrected for these reduced e.e. ratios, to represent the enantiopure values for PECD.

The importance of the quality of the circular polarization needs also to be highlighted because the measured b_1 is directly proportional to S_3. A low absolute value of S_3 will at best—when it is known—lead to a decreased sensitivity to chirality by increasing the error bar on b_1 and, at worst—if not recognized—lead to incorrect PECD amplitudes. The argument must be also extended to cases where the Stokes parameters S_1 and S_2 defining respectively the linear polarization rates with respect to normal and 45° tilted

View Article Online
DOI: 10.1039/C6CP01293K

axis, are non-zero. In such cases, if the usual anisotropy parameter β is non-zero, the S_1 and S_2 contributions to the photoelectron angular distribution (PAD) need to be taken into account. This would be a severe issue in the case of a VMI spectrometer relying on Abel inversion of a 2D image (i.e. without electron time-of-flight available to provide a direct 3D momentum determination) since only the cases where the axis of symmetry given by the light's polarization state is contained within the detector plane can be properly treated. However, in the case of the present experiments, the DESIRS beamline delivers quasi-perfect CPL and the undesirable effects cited above do not apply here. Also, the error bars on the S_3 measurement are negligible and do not increase those of b_1.

The data shown in Figs. 1 and 2 can be obtained at different photon energies in order to study dynamical effects such as the dependence on electron kinetic energy or the effects of continuum resonances. For this, the orbital-specific PECD has been extracted by taking the PES intensity weighted average of b_1 over the FWHM of the corresponding electronic band. The results are given in Figures 3 and 4 for the HOMO and HOMO-1 of camphor, which also compile the data from previous works. The HOMO-1 data have been obtained by filtering the electron images on the sum of the camphor fragments (discarding therefore the parent contribution) and by considering the binding energy range 10.0–10.3 eV as in ref. [36]. Note that for the sake of providing highly accurate benchmarking PECD data, we list in Table 1 of the supplementary information (SI) the corresponding new b_1 values.

The new data on the HOMO orbital of camphor, as given by the solid squares in Fig.3, fit very well with previous existing data recorded below 10 eV and above 13 eV although they have much better accuracy. The completion of the 10–13 eV photon energy range is extremely useful since in this range the CMS-Xα model[36] made predictions of oscillations in the PECD which are now clearly evident in the experimental data. While these fixed equilibrium geometry calculations appear to overemphasize the magnitude of the swings experimentally observed in the 10–17 eV range, they do capture the essence of the energy dependent variation in b_1. One may speculate that allowance for vibrational motion averaging in such calculated PECD might attenuate the swing in b_1 values suggested by experiment. An alternative calculation, the density functional based B-spline model of Steiner et al. [41] has previously been reported and compared. In the case of core shell C1s ionization of camphor, both models give very comparable results in close agreement with the experimental data [41]. Unfortunately, due to limitations in the LB94 exchange-correlation potential employed for these B-spline calculations the scattering potential generated for the valence ionization was too attractive, and consequently the available B-spline model predictions do span this crucial first few eV above the HOMO ionization threshold.

In the case of the HOMO-1 orbital, as shown in Fig. 4, the new data in the 10–13 eV range display a reversed PECD asymmetry, as compared to the HOMO orbital, as the b_1 parameter flips sign. This experimentally observed behavior is well reproduced by the CMS-Xα model calculations until, in the first eV above threshold, the model predicts a spurious unobserved swing in b_1. Such low energy electrons will, of course be especially sensitive to the subtleties of the molecular potential, making this region especially challenging for calculation. Nevertheless, the overall experiment/theory is satisfactory.

3.2 Fenchone data

View Article Online
DOI: 10.1039/C6CP01293K

In Figures 5 and 6 we present photon energy dependent PECD data for the HOMO and the HOMO-1 orbital ionizations of fenchone, obtained following a similar procedure outlined for camphor. In particular, the same PEPICO filtering treatment, to decipher the HOMO and HOMO-1 contribution has been applied to fenchone since the two molecules exhibit the same fragmentation pattern with HOMO orbital ionization leaving an intact molecular ion, while the inner orbitals leads to the cation fragmentation.

Pre-alerted by previous reports [25, 37] that similarly sourced commercial fenchone samples may not be enantiopure, and by our own experience with camphor (above), we took additional steps to verify purity of our fenchone samples. The two different enantiomeric samples of fenchone were analyzed by GC×GC-TOFMS to obtain a precise value of the e.e. The results of the chromatographic analysis are shown in Table 1. While the S-fenchone sample was perfectly enantiopure, the nominal R-fenchone sample, had an e.e. of 82.1 ±0.5 %. Note that here the error bars are given by the 3σ statistical distribution analysis of the e.e. measurements over 10 injections into the GC×GC-TOFMS apparatus.

While treating the fenchone PECD data we could infer such an enantiopurity difference between the two samples of fenchone since at the three photon energies for which we had measured the PECD for both enantiomers (9.4, 15.5 and 18.6 eV) we observed systemically lower magnitudes for the b_1 values of the R-sample. The average ratio of the b_1 absolute values for the R-, S- enantiomer pairs at these three photon energies, weighted by the standard deviation, provides us with e.e.[R]/e.e.[S] ratio of 0.82±0.01, as deduced from data presented in Fig. S1(b), in perfect agreement to the 0.821±0.005 obtained from the GC×GC-TOFMS analysis (see Table 1). All the new data presented here in figures (and including Table 2 SI) have been corrected for the reduced sample enantiopurity, as was done earlier with our camphor data.

In a more extensive study using REMPI-PECD Lux et al. [52] have similarly demonstrated relative e.e. determinations with better than 1% uncertainty for fenchone mixtures spanning the full range (0–100 %). However, as compared to this latter method, the i^{2}PEPICO experiment provides the capability for ion mass-tagged PECD measurement. This allows for the simultaneous enantiomer specific analysis of multi-component mixtures which was proposed and demonstrated for a mixture of chiral and non-chiral species - spurious achiral decomposition product of alanine[15] - and for prepared mixtures of chiral compounds by Rafie Fanood et al. [30]. In that later case an e.e. measurement on a component present in chiral mixture was made with 20 % uncertainty, the limitation being the restricted data rate in that work. The present result confirms that this is not a fundamental restriction and that mass-selected PECD can be used for analyzing gas phase enantiomeric excess with precision in the ±1 % range. This is not far below chiral chromatographic measurement precision and very competitive with other gas phase chiroptical methods for relative ee determination, such as the one based upon microwave three-wave mixing [33, 53]. Note that in addition, PECD-PICO may as well provide the chemical purity (by MS-TOF analysis of the coincident cation) at the same time as the relative enantiopurity for each mass-selected species (by PECD).

The new measurements provide b_1 data for fenchone below 12 eV photon energy, where previously none had been published. The CMS-Xα modeling predicts for the HOMO orbital (Fig. 5) an intense asymmetry in the first few eVs kinetic energy (KE) range, followed by a sign change of the asymmetry at increasing photon energies. These

View Article Online
DOI: 10.1039/C6CP01293K

features are reproduced by the experimental data. However, and unlike the clearer case of camphor, the situation of the "HOMO-1" orbital in fenchone (Fig. 6) is more complex since due to our limited electron energy resolution and to the congestion of the PES, what we labeled as "HOMO-1" is in fact a mixture of several closely lying electronic orbitals such as the one labeled 39, 40 and 41 in Ref. [40]. In consequence the b_1 value observed in the A band (10.05–10.61 eV binding energy range) represents a blend of these individual ionizations. The comparison with the theoretical modelling of the various contributing orbitals is consequently not straightforward, although at high energy all calculations agree toward the same sign of b_1, corresponding to the experimental observations i.e. fixing the absolute configuration.

3.3 Camphor/fenchone comparison : sensitivity to isomerism

The sensitivity of PECD to chemical substitution in oxirane derivatives has been studied in the past theoretically [16] as well as experimentally [17] and strong effects upon substitution were reported even when the initial orbital appeared identical for all molecules and not centered onto the substituted chemical group. Even more spectacular are effects, as seen here, concerning pure isomers with the same chemical formula and the same localization of the HOMO orbitals as shown in Fig. S2. In this respect, Powis et al. [40] already commented on the different PECD values measured on camphor and fenchone, albeit in an energy range restricted to electron KE > 4 eV for the HOMO orbital. Here we can now extend this comparison to the threshold energy regions, which are known to be the most sensitive to the molecular potential [7]. The HOMO orbital in both molecules is a localized 2p lone pair of the carbonyl oxygen (see Fig. S2). The corresponding hole in the unrelaxed cation potentials used for the CMS-Xα calculations is consequently similarly localized. The good CMS-Xα theory/experiment agreement that is evident, even within a few eV of the ionization threshold (Figs 3, 5) is then possibly attributable to relative accuracy with which the atomic-site partitioning of the multiple scattering potential model can reproduce this potential. Supporting this, ionization of the highly localized C1s orbital by soft X-ray SR in early studies of camphor and fenchone is similarly well described by the CMS-Xα calculations. In contrast, the more delocalized HOMO-1 ionizations give rise to PECD behavior which as discussed above is less well described by the CMS-Xα calculations in the low energy region.

Turning to a broader comparison of these molecules, both are rigid single-conformer structures whose isomerism can be reduced to the shift of two methyl groups (see Scheme 1) from a top position to a side one, none of them being directly connected to the asymmetric carbons (C1, C4) nor to the carbonyl group — in other words the isomeric changes are remote from the chiral centers and the localized HOMO orbitals. Figure 7 shows the PES and PECD obtained at photon energies of 10.3 and 10.5 eV for 1R,4R-(+)-camphor and 1R,4S-(–)-fenchone respectively. The two photon energies are close enough so that dynamical effects would be marginal, so we can compare directly the data. The figure shows similar PES for both molecules, except for an energy shift due to the small ionization energy difference (fenchone is 180 meV lower than camphor[40, 51]). The PECD curves, however, show a striking difference with opposite sign for the same absolute configuration of the two molecules. Here, note that absolute configuration of the C4 asymmetric carbon is fixed by the rigid cycle; the change in labelling from 4R (camphor) to 4S (fenchone) is due to a change in priority assigned by the Cahn-Ingold-Prelog nomenclature rules rather than a rearranged molecular configuration. Therefore, the natural comparison is shown in Fig. 7 and Scheme 1, i. e. between 1R,4R-(+)camphor

View Article Online
DOI: 10.1039/C6CP01293K

and 1R,4S-(–)-fenchone. In this respect the quasi-mirroring of the PECD curves appearing in Fig. 3 is quite spectacular since it shows, that at 10.3/10.5 eV photon energy the two isomers behave nearly as opposite enantiomers while they have in fact the same absolute configuration!

A marked difference between REMPI-PECD measurements on fenchone and camphor at a single given energy was also reported by Lux et al. [24, 25], especially for the odd C_n (n>1) parameters describing the high-order multi-photon electron angular distribution. Of course the role of the intermediate resonant state adds additional complexity to the interpretation of such results. Indeed, in the REMPI-PECD case, the origin may also lie in the resonant excited intermediate state which can also differently select, and align, the two isomers. Such a structure-specificity in REMPI experiments is a well known process which has been recently applied to measure conformer-specific response in absorption CD [54]. In the present work, the b_1 sign inversion makes this isomerism phenomenologically quite striking but its origin is also very clear being, in a one-photon ionization regime, purely due to the multiple scattering of the outgoing electron in the chiral potential of the molecule.

The comparison between 1R-camphor and 1R-fenchone PECD spectra is shown across the full photon energy range studied in Figure 8 and Figure 9 for respectively the first ($HOMO^{-1}$ channel) and second PES bands. In a previous study carried out with photon energies above 13 eV[40], a difference between the b_1 curve for the HOMO orbitals of fenchone versus camphor was observed mainly as a difference in amplitude in the 18-22 eV range, ie KE of ~ 9–13 eV, corresponding to a shape resonance. These are known to be sensitive to molecular structures. Here (Fig. 8) the new PECD data show a far more striking signature of isomerism, in the KE=0–5 eV region. Although it is also quite evident in the A band PECD (Fig. 9), this enhanced sensitivity is especially marked for electrons ejected from the HOMO orbital. There is a totally different behavior of the b_1 parameter, in terms of oscillation pattern and sign, for the same absolute configuration. With caveats discussed above, b_1 is very well reproduced by the CMS-Xα modeling.

In a more general context the enhanced sensitivity of the chiral parameter b_1 to the molecular potential—and thus to effects such as isomerism, chemical substitution, conformers, vibrational dynamics, clustering—has been discussed previously [3, 6, 7] and arises from the strong dependence on the phase shifts of the different outgoing partial waves that interfere in the scattering process[5]. This dependency has been shown to be much more marked in the dichroic parameter b_1 than in the anisotropy parameter β or in the cross section[16], so that tiny changes in the molecular potential will have a much larger effect on this new observable (b_1) accessible on randomly-oriented chiral targets. In contrast to b_1, numerical computations of the β parameter of fenchone[40] and camphor[41] lead to very similar, non-distinguishable behaviour with photon energy. The present results also confirm that the enhanced sensitivity of PECD to the molecular potential is especially marked for slow electrons as already pointed out in the case of conformers[14, 15] and dimers [18]. Finally, this sensitivity to isomerism confirms also that PECD is a long-range effect, at least for slow electrons, since in the case of camphor the methyl groups are localized quite far from the site of the ionized orbital.

Because PECD happens during the scattering process, it also observed upon inner-shell ionization from spherical orbitals, and some difference have also been found in the PECD

View Article Online
DOI: 10.1039/C6CP01293K

from C1s ionization of camphor and fenchone[55]. However these differences, mainly observed along the shape resonance above 10 eV KE, are much smaller than what is observed here for outer valence shell electrons. This difference of sensitivity to isomerism between core and valence ionization, clearly observed experimentally and simulated by theory, is a priori unexpected since in both cases the initial orbital is very localized, and in the same area in the molecule.

In a broader context of chiroptical spectroscopies, note that the micro-wave 3 wave-mixing technique has been shown to be also sensitive to isomerism able for instance to distinguish menthone from isomenthone[56].

4. Conclusions and future prospects

In this work we have experimentally studied the chiroptical PECD effect induced by one-photon valence-shell ionization in the VUV range of randomly-oriented enantiomers. We provide b_1 values on showcase chiral isomers camphor and fenchone with high accuracy since sources of systematic errors such as imperfect CPL or enantiopurity have been taken into account. We expect these data to be useful for the development and benchmarking of new PECD experiments, especially those involving VUV radiation based upon HHG and probably in the near future Free Electron Lasers (FELs).

In addition, in the context of a growing development of VUV/XUV CPL sources from FELs[57], HHG[29, 58, 59], plasma-based laser[60] and associated polarizing optics[61], PECD could, like other dichroic effects [62], be used as a "molecular polarimeter template", especially when either the β parameter is null or known, or when the linear polarization components of light (S_1 and S_2) are negligible, in which case accurate PECD benchmarking with the present data would allow the disentangling of the unpolarized component (S_4) from the circular one (S_3). This would be a complementary approach from the molecular polarimetry data deduced from molecular-frame photoelectron angular distributions (MF-PADs), recently demonstrated [63] and valid in the dissociative ionization continuum range of small molecules, i.e., above 20 eV or so. We therefore hope in this context, to contribute to the expansion of the active field of polarization dependent short wavelength photodynamics with short pulses.

In the more fundamental context of the understanding of the PECD process itself, we found a remarkable agreement between the experimental data and the CMS-Xα modeling of the HOMO orbital of both camphor and fenchone, even in the challenging low KE energy range. On the other hand some clear discrepancies remain. Owing to the size and lack of symmetry simplifications in these molecules, current methods rely on solving independent electron dynamics in single reference derived potential (either semi-empirical as in CMS-Xα or DFT as in the B-spline method [41]. Future developments are likely to introduce electron correlations into the N-1 electron potential model, and the current experimental data could serve as a benchmark for judging performance of such developments. Equally, there is accumulating evidence of the need to take fuller account of vibrational motions in refining out understanding of PECD [21], something which is absent from the current capabilities of fixed-geometry computations.

Besides, the accuracy of the data we provide is such that limited departure from perfect enantiopurity in the samples we purchased could be detected, by the non-perfect mirroring of the R/S PECD data. The benchmarking versus a conventional

View Article Online
DOI: 10.1039/C6CP01293K

chromatographic analytical method, highlights the interest and high accuracy, in the % range, of PECD as a precise enantiomeric analytical tool in the gas phase. Especially when combined in with TOF mass spectrometry of the photoions, recorded in coincidence with the photoelectrons, via the so-called PECD-PICO scheme, we stress the ability to analyze a mixture of compounds simultaneously and to provide highly accurate relative ee measurement of each of these compounds, now with significantly improved accuracy over the first demonstrations of this capability [15, 30]. As compared to the well-established GC type of technique, PECD is a direct method with no derivatization, nor use of reagents, directly applicable in the gas phase, and which provides additional electronic information, as a multi-dimensional chiroptical probe (photon energy, electron energy, coincident ion mass). Also as compared to the REMPI-PECD-PICO technique, there is no need here, in the VUV one-photon PECD-PICO approach for any chromophore absorbing in the UV range, so that the method is genuinely universal. We intend therefore in the near future to apply such a PECD-PICO scheme to disentangle the enantiomeric composition of a complex mixture of samples.

Finally, our experimental data show a very striking signature of the profound sensitivity of PECD to isomerism with large and opposite asymmetries measured on the HOMO orbital of the same enantiomers of camphor and fenchone. This feature, especially marked for slow electrons, is very well reproduced by theory, while the same theory shows that the two isomers have similar anisotropy parameter β. This ability of PECD could be applied in the future in the field of gas phase chemical reactivity, in order to probe and disentangle isomers in chemical reactions involving chiral products, as for instance in combustion of biofuels. PECD, with its exquisite sensitivity to isomers would be, in this context of gas phase chemical reactions probed by photoionization, an additional observable to products appearance energies [64], or even to the full PES of mass-selected species [65, 66].

Acknowledgments

We are grateful to the general SOLEIL staff for running smoothly the facility under proposal 99150018 and 20140138. We also want to thank J.-F. Gil, J. Kruger and X. Tang for their help on the SAPHIRS experimental chamber.

View Article Online
DOI: 10.1039/C6CP01293K

Table 1: GC×GC-TOFMS analysis of the supplied fenchone samples, along with the relative e.e. measured by PECD.

	GC×GC-TOFMS			PECD
Sample	**Enantiomeric excess (%)**	**Chemical purity (%)**[b]	$\lvert e.e._R / e.e._S \rvert$	$\lvert e.e._R / e.e._S \rvert$
R-(+)-Camphor	+96.7 ± 0.9[a]	> 99.9	0.979(9) [a]	0.97(2) [c]
S-(–)-Camphor	–98.7 ±0.1[a]	> 99.9		
R-(–)-Fenchone	+82.1 ± 0.5[a]	> 99.9	0.821(5) [a]	0.82(1) [c]
S-(+)-Fenchone	–99.90 ±0.03[a]	> 99.9		

[a] 3σ error bars

[b] Non considering non-volatile or solvent species

[c] 1σ error bars

View Article Online
DOI: 10.1039/C6CP01293K

References

1. B. Ritchie, *Phys. Rev. A*, 1976, **13**, 1411-1415.
2. I. Powis, *J. Phys. Chem. A*, 2000, **104**, 878-882.
3. I. Powis, *J. Chem. Phys.*, 2000, **112**, 301-310.
4. N. Böwering, T. Lischke, B. Schmidtke, N. Müller, T. Khalil and U. Heinzmann, *Phys. Rev. Lett.*, 2001, **86**, 1187-1190.
5. I. Powis, *Adv. Chem. Phys.*, 2008, **138**, 267-329.
6. L. Nahon and I. Powis, in *Chiral recognition in the gas phase*, ed. A. Zehnacker, CRC Press - Taylor & Francis, Boca Raton, 2010, pp. 1 - 26.
7. L. Nahon, G. A. Garcia and I. Powis, *J. Elec. Spec. Rel. Phen.*, 2015, **204**, 322-334.
8. N. Berova, K. Nakanishi and R. Woody, *Circular dichroism principles and applications*, Wiley-VCH, New York, 2nd edn., 2000.
9. S. Stranges, S. Turchini, M. Alagia, G. Alberti, G. Contini, P. Decleva, G. Fronzoni, M. Stener, N. Zema and T. Prosperi, *J. Chem. Phys.*, 2005, **122**, 244303.
10. D. Catone, M. Stener, P. Decleva, G. Contini, N. Zema, T. Prosperi, V. Feyer, K. C. Prince and S. Turchini, *Phys. Rev. Lett.*, 2012, **108**, 083001.
11. S. Turchini, D. Catone, G. Contini, N. Zema, S. Irrera, M. Stener, D. Di Tommaso, P. Decleva and T. Prosperi, *ChemPhysChem*, 2009, **10**, 1839-1846.
12. S. Turchini, D. Catone, N. Zema, G. Contini, T. Prosperi, P. Decleva, M. Stener, F. Rondino, S. Piccirillo, K. C. Prince and M. Speranza, *ChemPhysChem*, 2013, **14**, 1723-1732.
13. G. Garcia, L. Nahon, C. J. Harding and I. Powis, *Phys. Chem. Chem. Phys.*, 2008, **10**, 1628-1639.
14. G. Garcia, H. Soldi-Lose, L. Nahon and I. Powis, *J. Phys. Chem. A*, 2010, **114**, 847.
15. M. Tia, B. Cunha de Miranda, S. Daly, F. Gaie-Levrel, G. A. Garcia, L. Nahon and I. Powis, *J. Phys. Chem. A*, 2014, **118**, 2765-2779.
16. M. Stener, G. Fronzoni, D. Di Tommaso and P. Decleva, *J. Chem. Phys.*, 2004, **120**, 3284-3296.
17. G. A. Garcia, H. Dossmann, L. Nahon, S. Daly and I. Powis, *Phys Chem Chem Phys*, 2014, **16**, 16214-16224.
18. L. Nahon, G. Garcia, H. Soldi-Lose, S. Daly and I. Powis, *Phys. Rev. A*, 2010, **82**, 032514.
19. S. Daly, I. Powis, G. A. Garcia, H. Soldi-Lose and L. Nahon, *J. Chem. Phys.*, 2011, **134**, 064306.
20. I. Powis, S. Daly, M. Tia, B. Cunha de Miranda, G. Garcia and L. Nahon, *Phys Chem Chem Phys*, 2014, **16**, 467-476.
21. G. Garcia, L. Nahon, S. Daly and I. Powis, *Nature Communications*, 2013, **4**, 2132
22. I. Powis, *J Chem Phys*, 2014, **140**, 111103.
23. M. H. Janssen and I. Powis, *Phys Chem Chem Phys*, 2014, **16**, 856-871.
24. C. Lux, M. Wollenhaupt, T. Bolze, Q. Q. Liang, J. Kohler, C. Sarpe and T. Baumert, *Angew. Chem.-Int. Edit.*, 2012, **51**, 5001-5005.
25. C. Lux, M. Wollenhaupt, C. Sarpe and T. Baumert, *ChemPhysChem*, 2015, **16**, 115-137.
26. C. S. Lehmann, N. B. Ram, I. Powis and M. H. Janssen, *J Chem Phys*, 2013, **139**, 234307.
27. M. M. Rafiee Fanood, I. Powis and M. H. Janssen, *J. Phys. Chem. A*, 2014, **118**, 11541-11546.

28. M. M. Rafiee Fanood, M. H. Janssen and I. Powis, *Phys Chem Chem Phys*, 2015, **17**, 8614-8617.
29. A. Ferré, C. Handchin, M. Dumergue, F. Burgy, A. Comby, D. Descamps, B. Fabre, G. A. Garcia, R. Géneaux, L. Merceron, E. Mével, L. Nahon, S. Petit, B. Pans, D. Staeder, S. Weber, T. Ruchon, V. Blanchet and Y. Mairesse, *Nature Photonics*, 2015, **9**, 93-98.
30. M. M. Fanood, N. B. Ram, C. S. Lehmann, I. Powis and M. H. Janssen, *Nat Commun*, 2015, **6**, 7511.
31. D. Patterson, M. Schnell and J. M. Doyle, *Nature*, 2013, **497**, 475-477.
32. D. Patterson and J. M. Doyle, *Phys Rev Lett*, 2013, **111**, 023008.
33. V. A. Shubert, D. Schmitz, D. Patterson, J. M. Doyle and M. Schnell, *Angew. Chem. Int. Ed. Engl.*, 2014, **53**, 1152-1155.
34. G. A. Garcia, L. Nahon, M. Lebech, J. C. Houver, D. Dowek and I. Powis, *J. Chem. Phys.*, 2003, **119**, 8781-8784.
35. T. Lischke, N. Böwering, B. Schmidtke, N. Muller, T. Khalil and U. Heinzmann, *Phys. Rev. A*, 2004, **70**, 022507.
36. L. Nahon, G. A. Garcia, C. J. Harding, E. A. Mikajlo and I. Powis, *J. Chem. Phys.*, 2006, **125**, 114309.
37. C. Lux, A. Senftleben, C. Sarpe, M. Wollenhaupt and T. Baumert, *Journal of Physics B: Atomic, Molecular and Optical Physics*, 2016, **49**, 02LT01.
38. R. Cireasa, A. E. Boguslavskiy, B. Pons, M. C. H. Wong, D. Descamps, S. Petit, H. Ruf, N. Thiré, A. Ferré, J. Suarez, J. Higuet, B. E. Schmidt, A. F. Alharbi, F. Légaré, V. Blanchet, B. Fabre, S. Patchkovskii, O. Smirnova, Y. Mairesse and V. R. Bhardwaj, *Nature Physics*, 2015, **11**, 654-658.
39. C. Loge and U. Boesl, *ChemPhysChem*, 2011, **12**, 1940-1947.
40. I. Powis, C. J. Harding, G. Garcia and L. Nahon, *ChemPhysChem*, 2008, **9**, 475-483.
41. M. Stener, D. D. Tommaso, G. Fronzoni, P. Decleva and I. Powis, *J. Chem. Phys.*, 2006, **124**, 024326.
42. I. Dreissigacker and M. Lein, *Phys. Rev. A*, 2014, **89**, 053406.
43. A. N. Artemyev, A. D. Muller, D. Hochstuhl and P. V. Demekhin, *J Chem Phys*, 2015, **142**, 244105.
44. C. Meinert and U. J. Meierhenrich, *Angew. Chem. Int. Ed. Engl.*, 2012, **51**, 10460-10470.
45. X. Tang, G. Garcia, G. Jean-Francois and L. Nahon, *Rev. Sci. Inst.*, 2015, **86**, 123108.
46. L. Nahon, N. de Oliveira, G. Garcia, J. F. Gil, B. Pilette, O. Marcouille, B. Lagarde and F. Polack, *J. Synchrotron Rad.*, 2012, **19**, 508-520.
47. B. Mercier, M. Compin, C. Prevost, G. Bellec, R. Thissen, O. Dutuit and L. Nahon, *J. Vac. Sci. Tech. A*, 2000, **18**, 2533-2541.
48. L. Nahon and C. Alcaraz, *Applied Optics*, 2004, **43**, 1024-1037.
49. G. Garcia, B. Cunha de Miranda, M. Tia, S. Daly and L. Nahon, *Rev. Sci. Inst.*, 2013, **84**, 053112.
50. G. A. Garcia, L. Nahon and I. Powis, *Rev. Sci. Inst.*, 2004, **75**, 4989-4996.
51. E. E. Rennie, I. Powis, U. Hergenhahn, O. Kugeler, G. Garcia, T. Lischke and S. Marburger, *J. Elec. Spec. Rel. Phen.*, 2002, **125**, 197-203.
52. A. Kastner, C. Lux, T. Ring, S. Zullighoven, C. Sarpe, A. Senftleben and T. Baumert, *ChemPhysChem*, 2016, DOI: 10.1002/cphc.201501067.
53. D. Patterson and M. Schnell, *Phys Chem Chem Phys*, 2014, **16**, 11114-11123.
54. A. Hong, C. M. Choi, H. J. Eun, C. Jeong, J. Heo and N. J. Kim, *Angew. Chem. Int. Ed. Engl.*, 2014, **53**, 7805-7808.

55. V. Ulrich, S. Barth, S. Joshi, U. Hergenhahn, E. Mikajlo, C. J. Harding and I. Powis, *Phys. Chem. A*, 2008, **112**, 3544-3549.
56. V. Alvin Shubert, D. Schmitz and M. Schnell, *J. Mol. Spec.*, 2014, **300**, 31-36.
57. E. Allaria, B. Diviacco, C. Callegari, P. Finetti, B. Mahieu, J. Viefhaus, M. Zangrando, G. De Ninno, G. Lambert, E. Ferrari, J. Buck, M. Ilchen, B. Vodungbo, N. Mahne, C. Svetina, C. Spezzani, S. Di Mitri, G. Penco, M. Trovó, W. M. Fawley, P. R. Rebernik, D. Gauthier, C. Grazioli, M. Coreno, B. Ressel, A. Kivimäki, T. Mazza, L. Glaser, F. Scholz, J. Seltmann, P. Gessler, J. Grünert, A. De Fanis, M. Meyer, A. Knie, S. P. Moeller, L. Raimondi, F. Capotondi, E. Pedersoli, O. Plekan, M. B. Danailov, A. Demidovich, I. Nikolov, A. Abrami, J. Gautier, J. Lüning, P. Zeitoun and L. Giannessi, *Physical Review X*, 2014, **4**, 041040.
58. D. D. Hickstein, F. J. Dollar, P. Grychtol, J. L. Ellis, R. Knut, C. Hernández-García, D. Zusin, C. Gentry, J. M. Shaw, T. Fan, K. M. Dorney, A. Becker, A. Jaroń-Becker, H. C. Kapteyn, M. M. Murnane and C. G. Durfee, *Nature Photonics*, 2015, **9**, 743-750.
59. O. Kfir, P. Grychtol, E. Turgut, R. Knut, D. Zusin, D. Popmintchev, T. Popmintchev, H. Nembach, J. M. Shaw, A. Fleischer, H. Kapteyn, M. Murnane and O. Cohen, *Nature Photonics*, 2014, **9**, 99-105.
60. A. Depresseux, E. Oliva, J. Gautier, F. Tissandier, G. Lambert, B. Vodungbo, J. P. Goddet, A. Tafzi, J. Nejdl, M. Kozlova, G. Maynard, H. T. Kim, K. T. Phuoc, A. Rousse, P. Zeitoun and S. Sebban, *Phys Rev Lett*, 2015, **115**, 083901.
61. J. Schmidt, A. Guggenmos, M. Hofstetter, S. H. Chew and U. Kleineberg, *Opt. Express*, 2015, **23**, 33564.
62. T. Mazza, M. Ilchen, A. J. Rafipoor, C. Callegari, P. Finetti, O. Plekan, K. C. Prince, R. Richter, M. B. Danailov, A. Demidovich, G. De Ninno, C. Grazioli, R. Ivanov, N. Mahne, L. Raimondi, C. Svetina, L. Avaldi, P. Bolognesi, M. Coreno, P. O'Keeffe, M. Di Fraia, M. Devetta, Y. Ovcharenko, T. Moller, V. Lyamayev, F. Stienkemeier, S. Dusterer, K. Ueda, J. T. Costello, A. K. Kazansky, N. M. Kabachnik and M. Meyer, *Nat Commun*, 2014, **5**, 3648.
63. K. Veyrinas, C. Elkharrat, S. Marggi Poullain, N. Saquet, D. Dowek, R. R. Lucchese, G. A. Garcia and L. Nahon, *Phys. Rev. A*, 2013, **88**, 063411.
64. D. L. Osborn, P. Zou, H. Johnsen, C. C. Hayden, C. A. Taatjes, V. D. Knyazev, S. W. North, D. S. Peterka, M. Ahmed and S. R. Leone, *Rev. Sci. Instrum.*, 2008, **79**, 104103.
65. A. Bodi, P. Hemberger, D. L. Osborn and B. Sztáray, *The Journal of Physical Chemistry Letters*, 2013, **4**, 2948-2952.
66. J. Kruger, G. A. Garcia, D. Felsmann, K. Moshammer, A. Lackner, A. Brockhinke, L. Nahon and K. Kohse-Hoinghaus, *Phys Chem Chem Phys*, 2014, **16**, 22791-22804.

View Article Online
DOI: 10.1039/C6CP01293K

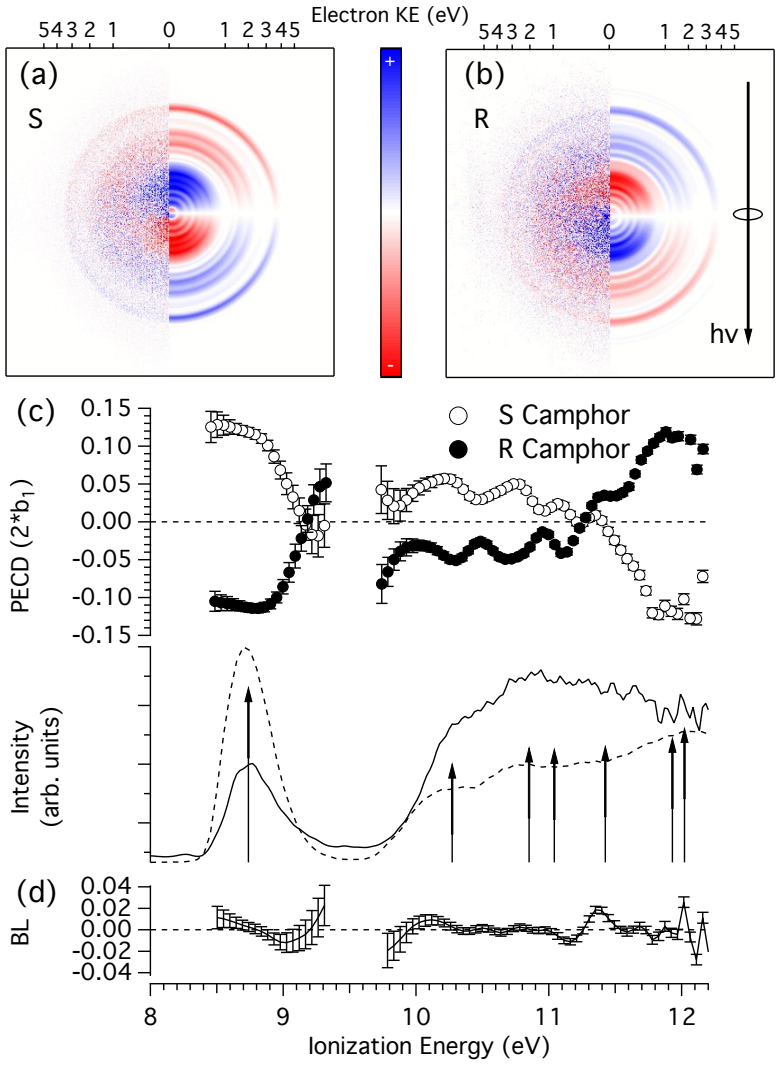

Fig 1 VMI difference images (LCP-RCP) recorded at *hv*=12.3 eV for 1S,4S-camphor (a) and 1R,4R-camphor (b) enantiomers. The left-half images show raw 2D-projections, and the right half the corresponding Abel inverted image (c) PECD (open and filled circles) and PES (solid line) extracted from inversion of the total and difference images. For clarity, the PECD is only shown for energies where the PES signal is higher than 10% of the maximum. The data have been normalized by S_3 and the e.e. measured by GC×GC-TOFMS. (d) PECD baseline (BL) obtained as the mean value of the S and R PECD curves. Error bars are obtained according to the description written at the end of the experimental section. A higher resolution PES obtained at *hv*=95 eV is also represented (dashed line) along with the calculated values (arrows), both taken from Ref. [51].

View Article Online
DOI: 10.1039/C6CP01293K

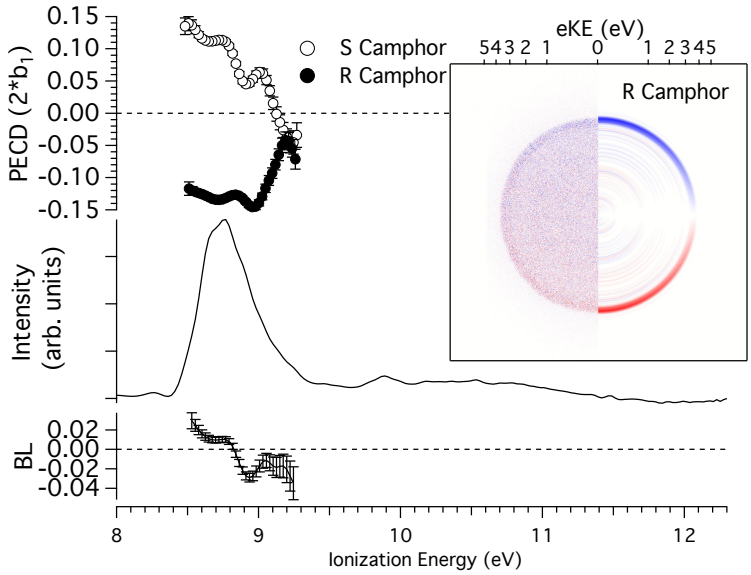

Fig 2 PECD (open and filled circles) and PES (solid line) extracted in coincidence with parent ions (m/z 152, plus 153 and 154 to take into account the ^{13}C contributions) recorded for 1R,4R- and 1S,4S-camphor at $h\nu$=12.3 eV. The data have been normalized by S_3 and the e.e. measured by GC×GC-TOFMS. The bottom-left axis represents the PECD baseline (*BL*) extracted as the mean value of the R and S PECD curves. The inset shows the raw (left) and Abel inverted (right) difference image for 1R,4R-camphor corresponding only to photoelectrons correlated to parent ions.

View Article Online
DOI: 10.1039/C6CP01293K

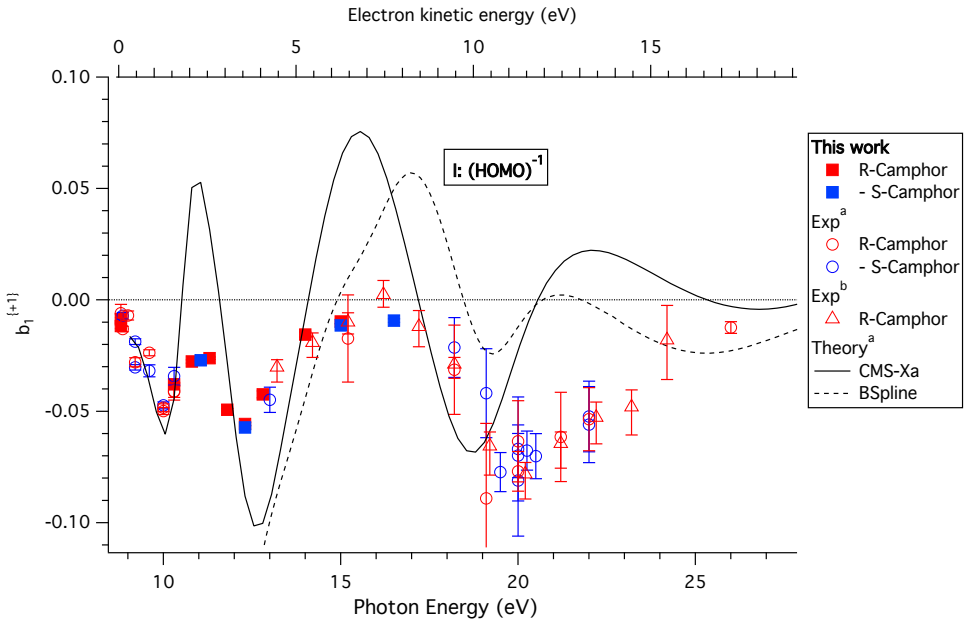

Fig 3 Mean chiral parameter (b_1) for ionization of the HOMO orbital of camphor obtained at different photon energies. The markers represent experimental measurements while the lines correspond to two different scattering models. The S-enantiomer data have been negated. For some of the data points, the statistical error bars are not visible because they are smaller than the point width (see table S1). The values in this work have been normalized by S_3 and the e.e. measured by GC×GC-TOFMS.

[a]From Ref. [36]

[b]From Ref. [35]

View Article Online
DOI: 10.1039/C6CP01293K

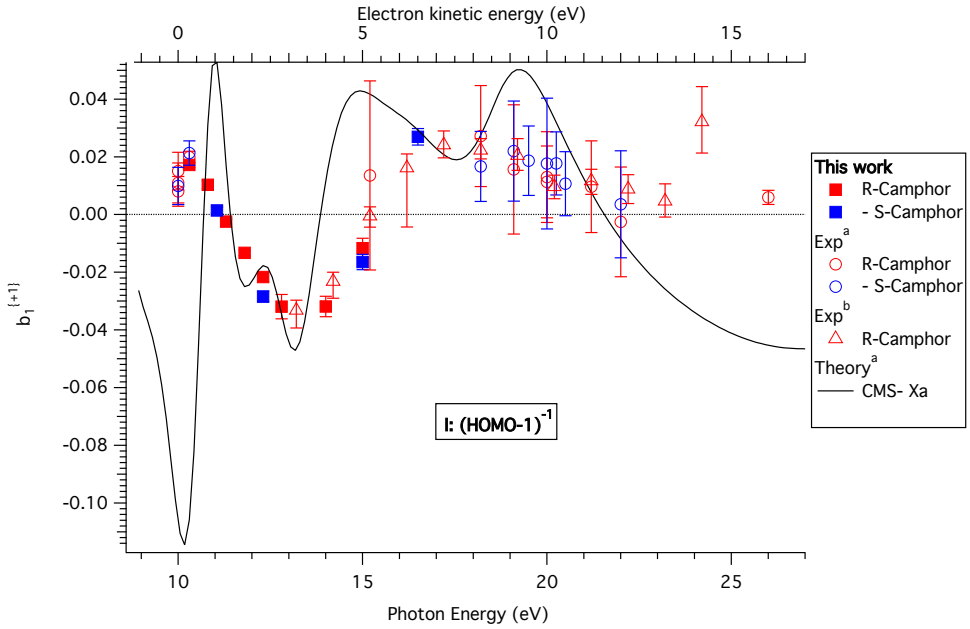

Fig 4 Mean chiral parameter (b_1) for ionization of the HOMO-1 orbital of camphor, corresponding to the binding energy region 10–10.3 eV, obtained at different photon energies. The markers represent experimental measurements while the line correspond to the CMS-Xα scattering models. The S-enantiomer data have been negated. For some of the data points, the statistical error bars are not visible because they are smaller than the point width (see table S1). The values in this work have been normalized by S_3 and the e.e. measured by GC×GC-TOFMS.

[a]From Ref. [36]

[b]From Ref. [35]

View Article Online
DOI: 10.1039/C6CP01293K

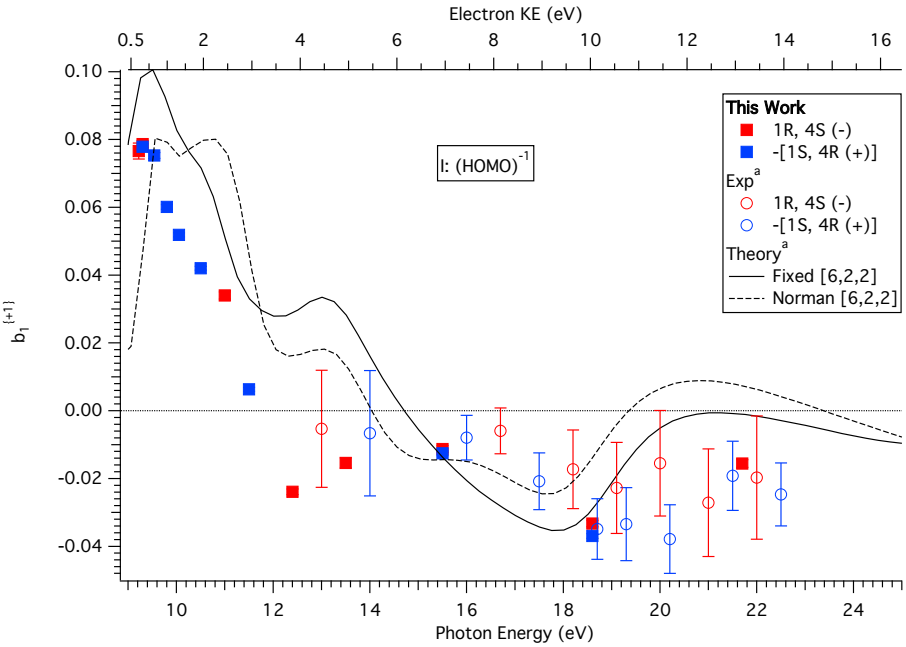

Fig 5 Mean chiral parameter (b_1) for ionization of the HOMO orbital of fenchone obtained at different photon energies. The values in this work are normalized to S_3 and to the absolute e.e. as provided by GC×GC-TOFMS. The markers represent experimental measurements while the lines correspond to two different CMS-Xα models. The S-enantiomer data have been negated. For some of the data points, the statistical error bars are not visible because they are smaller than the point width (see table S2).

[a]From Ref. [40]

View Article Online
DOI: 10.1039/C6CP01293K

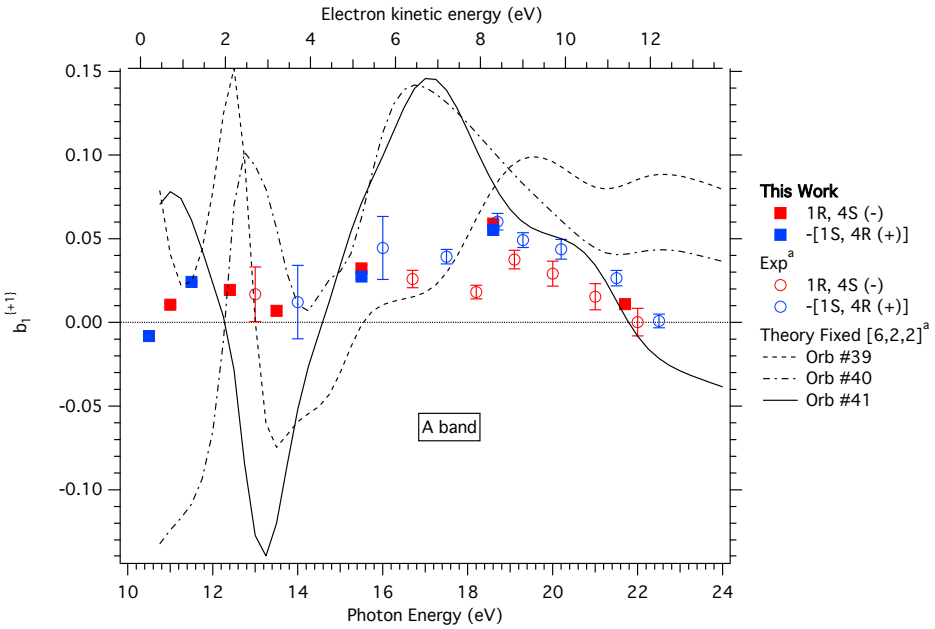

Fig 6 Mean chiral parameter (b_1) of the A band, corresponding to the binding energy region 10.05-10.61 eV of fenchone obtained at different photon energies. The data in this work are normalized to S_3 and to the absolute ee as provided by GC×GC-TOFMS. The markers represent experimental measurements while the lines correspond to two different CMS-Xα models. The S-enantiomer data have been negated. For some of the data points, the statistical error bars are not visible because they are smaller than the point width (see table S2).

[a]From Ref. [40]

View Article Online
DOI: 10.1039/C6CP01293K

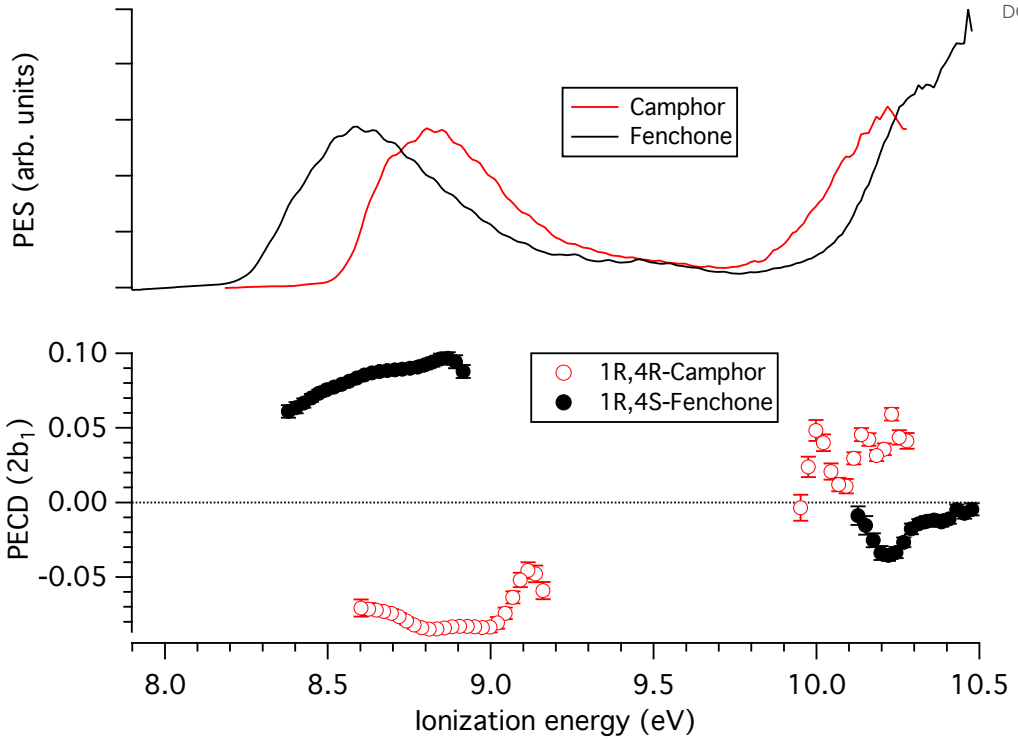

Fig 7 PES and PECD for R-camphor (red) and R-fenchone (black) recorded at *hv*=10.3 eV and 10.5 eV respectively. The data have been normalized to S_3 and the absolute e.e. as provided by GC×GC-TOFMS.

View Article Online
DOI: 10.1039/C6CP01293K

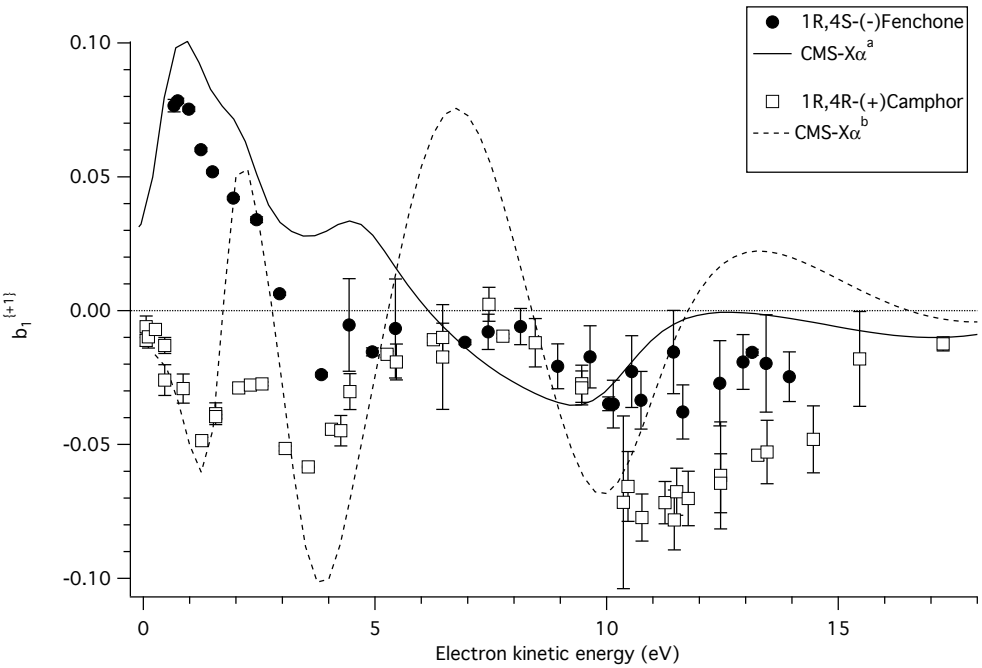

Fig 8 Chiral parameter ($b_1^{\{+1\}}$) for ionization from the HOMO orbital of R-fenchone and R-camphor (S enantiomers negated). The points represent all the available experimental data in the literature, including the present work, while the lines correspond to CMS-Xα calculations. The data have been normalized to the absolute e.e. as provided by GC×GC-TOFMS.

[a]From Ref. [40]

[b]From Ref. [36]

View Article Online
DOI: 10.1039/C6CP01293K

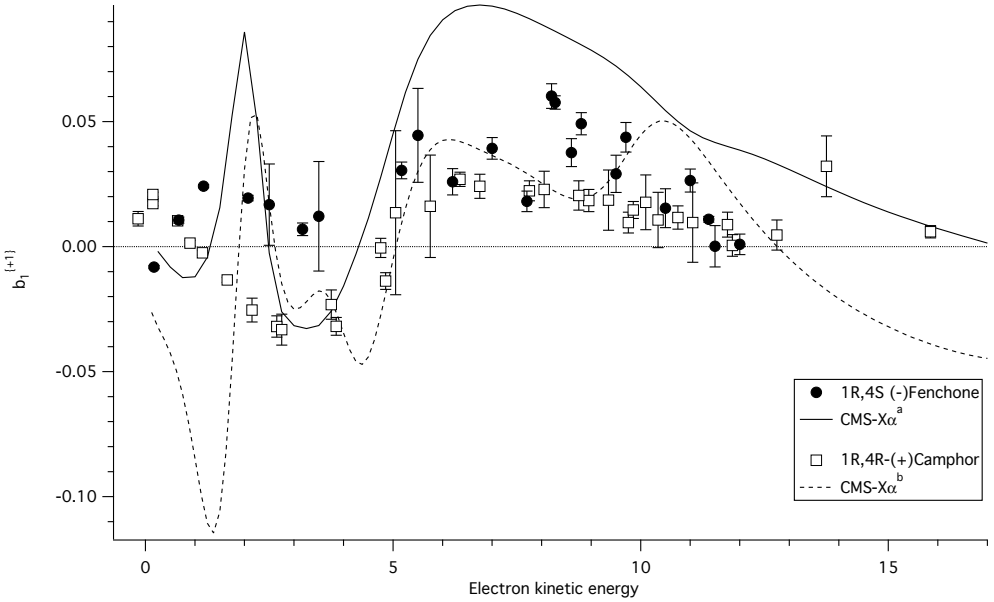

Fig 9 Chiral parameter (b_1) for the A region of R-fenchone and ionization from the HOMO-1 orbital of R-camphor. The points represent all the available experimental data in the literature (S enantiomers negated), including the present work, while the lines correspond to CMS-Xα calculations. In the case of fenchone, an average theoretical curve of three orbitals (#39,#40 and #41) weighted by their cross sections is shown. The data have been normalized to the absolute e.e. as provided by GC×GC-TOFMS.

[a]From Ref. [40]

[b]From Ref. [36]